Analyst

PAPER

Cite this: *Analyst*, 2020, **145**, 7932

Graphene/gold nanoparticle composites for ultrasensitive and versatile biomarker assay using single-particle inductively-coupled plasma/mass spectrometry†

Yuqian Xing, Juan Han, Xu Wu, David T. Pierce * and Julia Xiaojun Zhao*

Received 20th May 2020,
Accepted 24th September 2020

DOI: 10.1039/d0an01019g

rsc.li/analyst

An ultrasensitive and versatile assay for biomarkers has been developed using graphene/gold nanoparticles (AuNPs) composites and single-particle inductively-coupled plasma/mass spectrometry (spICP-MS). Thrombin was chosen as a model biomarker for this study. AuNPs modified with thrombin aptamers were first non-selectively adsorbed onto the surface of graphene oxide (GO) to form GO/AuNPs composites. In the presence of thrombin, the AuNPs desorbed from the GO/AuNPs composites due to a conformation change of the thrombin aptamer after binding with thrombin. The desorbed AuNPs were proportional to the concentration of thrombin and could be quantified by spICP-MS. By counting the individual AuNPs in the spICP-MS measurement, the concentration of thrombin could be determined. This assay achieved an ultralow detection limit of 4.5 fM with a broad linear range from 10 fM to 100 pM. The method also showed excellent selectivity and reproducibility when a complex protein matrix was evaluated. Furthermore, the diversity and ready availability of ssDNA ligands make this method a versatile new technique for ultrasensitive detection of a wide variety of biomarkers in clinical diagnostics.

1. Introduction

Graphene oxide (GO) has been widely applied for fluorescence-based bioassays due to its unique optical properties.[1,2] In general, it is a high-capacity energy acceptor and has played a significant role as a quencher in the fluorescence resonance energy transfer (FRET) of optical bioassays.[3,4] For instance, single-stranded DNA (ssDNA) is easily adsorbed to the GO surface because of strong π–π stacking interactions between the base structure of ssDNA and the two-dimensional multi-hexagonal structure of GO.[5] The strong adsorption between GO and ssDNA, coupled with the excellent quenching ability of GO provides a sensitive fluorescence platform for detecting and determining the concentration of biomolecules.[6] Two major factors determine the sensitivity of DNA-sensing applications of this platform. The first factor is a target-induced DNA conformational change, which results in desorption of fluorophore molecules from the GO, and thus increased fluorescence signal. Since the first report by Lu *et al.* in 2009,[6] a broad range of targets including nucleotides,[7] metal ions,[8] proteins,[9] enzymes,[10] and other small molecules[11] have been detected using various ssDNA conformational changes with this platform.[12] The second factor is the emission output based on FRET between fluorophore molecules and the GO. However, the high background emission of some complex samples,[13] photobleaching of the fluorophores, and practical limitations of the fluorophotometers have prevented more than incremental improvements in optical sensitivity and therefore limited achievement of sub-picomolar detection. Thus, a better signaling method is needed to achieve these ultratrace detection limits.

Two possible strategies could improve the signal output and lower the detection limits of the GO platform. The first strategy is to introduce an amplification step in the sensing process.[14] Several of these methods have been applied for oligonucleotide amplification, such as polymerase chain reaction and other isothermal nucleic acid amplification methods.[15] However, specific enzymes and delicate sequence design were required, diminishing the assay feasibility or versatility. The second strategy is to utilize a more sensitive signaling scheme. A detection method can response to ultralow amount of the target, such as electrochemical sensors and surface-enhanced Raman spectroscopy.[16–18] Another candidate

Department of Chemistry, University of North Dakota, Grand Forks, North Dakota 58202, USA. E-mail: julia.zhao@und.edu, david.pierce@und.edu

†Electronic supplementary information (ESI) available: Instrument parameters of ICP-MS, zeta potential, TEM characterization of nanomaterials. SsDNA modification density on AuNPs, comparation of AuNPs quantification by two models of ICP-MS. See DOI: 10.1039/D0AN01019G

is the inductively coupled plasma-mass spectrometry (ICP-MS) when operated in a time-resolved mode with very short signal integration periods, called dwell times. This configuration has already demonstrated encouraging results for analysis of nanomaterials and is often referred to as single-particle ICP-MS (spICP-MS).[19–21] The method provides "particle by particle" measurements that include information about particle number concentration, particle size, and size distribution.[21] Each particle that enters the ICP plasma forms an ion cloud that results in an isotope count registered by the MS during a single dwell time measurement.[22,23] Although most spICP-MS applications to date have focused on the characterization and direct quantification of nanoparticles themselves,[24,25] the capacity for ultralow detection of the particle concentration also makes spICP-MS a promising tool for ultrasensitive bioassays.[26,27] Zhang *et al.* developed a multiple DNA assay using different isotopes of nanoparticles as the output signal. The nanoparticles were first captured by the heterogeneous sandwich structure and then melted and washout into the ICP-MS. The nanoparticle concentration quantified by spICP-MS was proportional to the concentration of the target.[28]

Considering the characteristics of ultrasensitive detection and methods with an ultralow detection limits (sub-picomolar),[14] the detection of ultralow concentrations of biomarkers, such as bloodborne viruses, circulating tumor cells, and circulating nucleic acids,[29] might be met by using spICP-MS measurements as the signaling system. Based on this hypothesis, we developed an ultrasensitive yet versatile graphene platform for detecting and quantifying the model biomarker thrombin using gold nanoparticles (AuNPs) and spICP-MS methods. Thrombin is a kind of serine protease that plays a crucial role in blood coagulation and is a biomarker for venous thrombosis, thrombophilia, abnormal coagulation, and hundereds of other disease states.[10,30,31] We fabricated a sensing platform based on GO/DNA recognition and spICP-MS detection of AuNPs coupled to that recognition. An ultralow detection limit of 4.5 fM was archived by the combination of excellent recognition ability of GO for ssDNA and single nanoparticle of spICP-MS. Moreover, the diversity and ready availability of ssDNA sequences that can be bound to AuNPs make then an excellent building block for various targets because they can work as an aptamer or as a complementary sequence.[32,33] Hence, our combined sensing platform and spICP-MS method has potential as a broad-spectrum bioassay for ultrasensitive detection of biomarkers in clinical diagnostics.

2. Experimental section

2.1. Materials and reagents

Gold nanoparticles (20 nm) were purchased from Cytodiagnostics Inc (Burlington, Canada). Gold standard solution was purchased from Inorganic Ventures (Christiansburg, VA). High purity liquid argon was used as the plasma gas and the nebulizer gas for all ICP-MS measurements. In the conventional ICP-MS measurements, an ultra-high purity helium gas was used to remove undesirable molecule ions in the kinetic energy discrimination (KED) mode. (11-Mercaptoundecyl) hexa (ethylene glycol) (TOEG6), tris(2-carboxyethyl)phosphine hydrochloride (TCEP), sodium chloride, magnesium chloride, sodium phosphate monobasic, sodium phosphate dibasic, sodium citrate tribasic dihydrate, bovine serum albumin (BSA), thrombin from human plasma and 0.22 μm filter membranes were purchased from Sigma-Aldrich (St Louis, MO). Immunoglobulin G (IgG) was purchased from Santa Cruz Biotechnology (Dallas, TX). Fetal bovine serum (FBS) was purchased from VWR (Radnor, PA). Single layer graphene oxide was purchased from ACS Material (Pasadena, CA). The deionized (DI) water (18.2 MΩ cm) was produced from a Millipore water purification system. All DNA sequences were synthesized by Integrated DNA Technology (Coralville, IA). The sequences[34] of DNA used were as follows:

m29: 5′-HS-$(CH_2)_6$-TTTTTAGTCCGTGGTAGGGCAGGTTGGGGTGACT

m29-F: 5′-HS-$(CH_2)_6$-TTTTTAGTCCGTGGTAGGGCAGGTTGGGGTGACT-Alex750-3′.

2.2. Instruments

UV-Vis absorption measurements were performed on a PerkinElmer Lambda 1050 UV/Vis/NIR spectrometer (PerkinElmer, Santa Clara, CA), equipped with a Peltier temperature control accessory. Zeta potential of nanomaterials was measured using Zetasizer nano (Malvern Panalytical, UK). Fluorescence spectra were obtained with an RF-6000 spectrophotometer (Shimadzu, Japan). Transmission electron microscopy (TEM) images of GO and AuNPs were taken using a Hitachi 7500 transmission electron microscope (Hitachi, Japan). All ICP-MS measurements were carried out using a Thermo Scientific iCAP Qc ICP-MS (Bremen, Germany) coupled with a 4-channel 12-roller peristaltic pump, nickel sample and skimmer cones, a Teledyne CETAC ASX560 autosampler (Omaha, NE), a microflow perfluoroalkoxy nebulizer (Thermo Scientific) and a Peltier-cooled quartz cyclonic spray chamber. To monitor the ICP-MS instrument, the THERMO-4AREV (Thermo Scientific) standard was run daily for maximum ^{59}Co, ^{238}U and minimum $^{140}Ce^{16}O/^{140}Ce$ signal. The ICP-MS measurements of AuNPs were controlled by the Qtegra™ software (version 2.8.2944.202). The instrument operating parameters used for the single particle and conventional ICP-MS measurements are listed in Table S1 (ESI†).

2.3. Preparation of ssDNA modified AuNPs

Thiol-functionalized ssDNA (SH-ssDNA) (100 μL of 200.0 μM) was reduced in the 100 μL of TCEP (20.0 mM), and then was incubated for 2 h at room temperature. The amount of ssDNA was quantified with UV-Vis spectrometry. The modification of AuNPs with ssDNA was performed according to the literature with a slight change.[35] Briefly, the reduced SH-ssDNA (10 μL of 100.0 μM) was mixed with 1.0 mL of 1 OD 20 nm-diameter AuNPs under vortexing for 1 min and was retained in the con-

tainer for 10 min at room temperature. Afterward, a 100 μL aliquot of citrate-HCl buffer (100 mM, pH 4.3) was added to adjust the pH of the solution and the mixture was incubated for 30 min, followed by a 50 μL addition of 300.0 μM TOEG6. After an additional 10 min of static incubation, the solution was centrifuged at 6500*g* for 30 min. The precipitates were collected and washed twice with DI water. The final pellet was re-dispersed in 1.0 mL of DI water and stored at 4 °C for further use.

2.4. Adsorption of ssDNA to GO

A 50 μL aliquot of 5×10^{11} particle per mL AuNPs-ssDNA and 50 μL of 400.0 μg mL^{-1} of GO were incubated in 1.0 mL of PBS buffer (10 mM with 0.5 mM $MgCl_2$, pH 7.4) at room temperature for 30 min with regular shaking. Then the solution was vacuum filtered through a 0.22 μm pore membrane. After washing twice with water and once with PBS buffer, the maroon-colored GO/AuNPs composites distributed on the membrane surface were re-dispersed in 2 mL of PBS buffer by using an ultrasonic water bath.

2.5. Analysis of thrombin by GO/AuNPs composites using spICP-MS

A 50 μL aliquot of thrombin solution with varied concentration was incubated with 50 μL of prepared GO/AuNPs composites in a total of 500 μL of PBS buffer (10 mM with 0.5 mM $MgCl_2$, pH 7.4) at 37 °C with regular shaking. After 1 h of incubation, the solution was removed by syringe and filtered using a 0.22 μm membrane. After 10 min of ultrasonic agitation in a water bath, the filtrate analyzed by spICP-MS.

3. Results and discussion

3.1. Design and function of the bioassay platform

The graphene-based sensing platform was based on spICP-MS direct-counting of AuNPs that desorb from a designed GO/AuNPs composite. Desorption is caused by a reaction between the target biomolecule and the ssDNA ligands (aptamer) modified on the surface of the AuNPs. The sequential design of this platform is illustrated in Scheme 1. First, a thrombin-selective aptamer (ssDNA sequence with strong affinity to thrombin) is covalently immobilized on the surface of 20 nm citrate stabilized AuNPs through the formation of an Au–S bond. After incubation with a GO sheet, the aptamer modified AuNPs are adsorbed on the surface of GO due to the strong π–π stacking interaction between the ring structures of ssDNA base and the GO sheet, thereby forming the GO/AuNPs composite (Scheme 1A). After thoroughly washing to remove any free AuNPs, the target biomolecule, thrombin, is introduced to the platform. In the presence of thrombin, aptamer on the AuNPs complexes with the thrombin molecule and changes the aptamer structure (Scheme 1B). This conformational change breaks the interaction between the aptamer and the GO, causing the associated AuNPs–aptamer to desorb from the GO surface. Before introducing the solution into the spICP-MS, it is filtered to remove the AuNPs still adsorbed to GO. In this way, only the desorbed, thrombin-complexed AuNPs are injected into the ICP-MS (Scheme 1C) and there should be no aptamer-modified AuNPs desorbed in the absence of thrombin (Scheme 1D). Individual AuNPs are detected in the single-par-

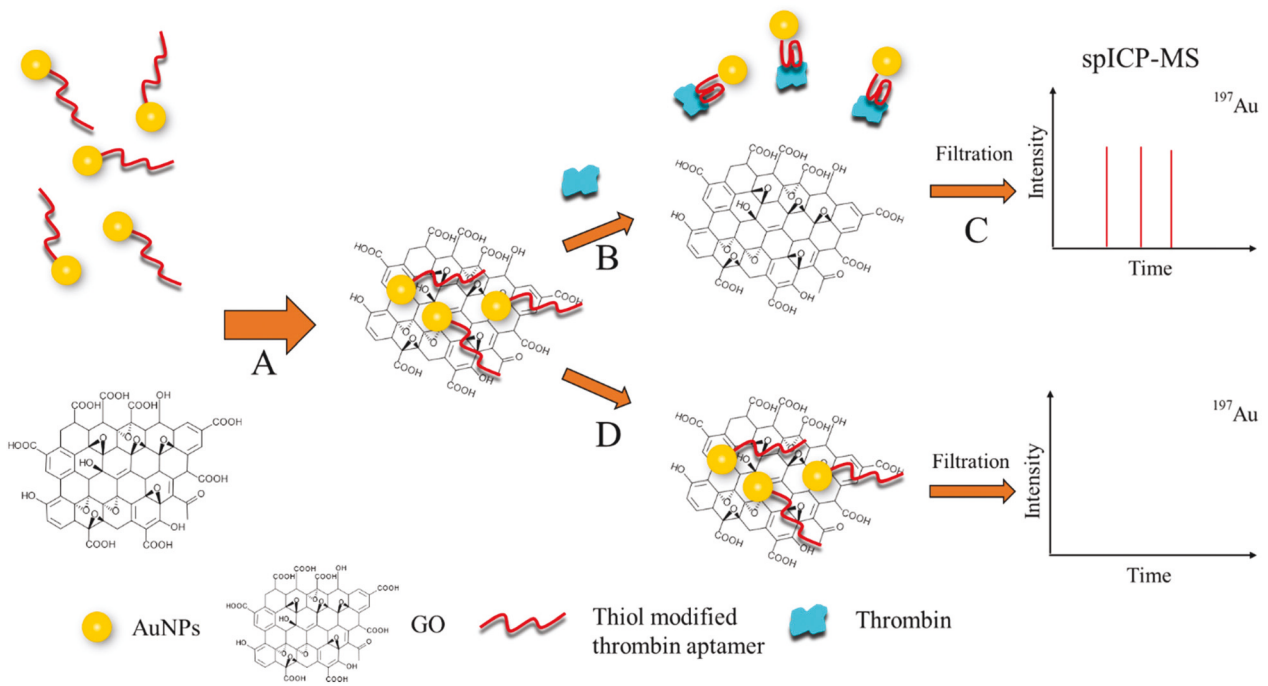

Scheme 1 Schematic illustration of thrombin detection using aptamer modified AuNPs by spICP-MS. A, Thrombin aptamer modified AuNPs incubated with GO; B, thrombin molecule as target incubated with GO/AuNPs composites; C, desorbed AuNPs were separated and introduced into spICP-MS; D, no thrombin molecule added as control.

ticle analysis mode as a measured count of $^{197}Au^{+}$ above a certain background threshold. The number of detected AuNPs are directly related to the number of AuNPs desorbed from GO by thrombin–aptamer complexation and also to the thrombin concentration. Because the spICP-MS method can easily detect even small number (<100) of AuNPs per mL of solution, this assay should be able to achieve ultralow detection limits for thrombin or other potential biomarkers.

3.2. Formation of GO/AuNPs composites

Two signaling modes have been used for the graphene/DNA based fluorescence bioassays. Both modes depend on the sequence of ssDNA adsorbed to the GO.[7,36] The "turn off" mode, also termed the post-adsorb strategy, requires incubation of the target molecule with dye modified ssDNA, followed by addition of GO to cause fluorescence quenching after the unbound ssDNA is adsorbed to the GO surface. The "turn on" mode, also termed the pre-adsorb strategy, requires initial adsorption of the dye modified ssDNA reagent to the GO surface in order to start with the fluorescence quenched. Subsequent addition of target molecules causes desorption of dye molecules from the GO platform due to the interaction with ssDNA, resulting in fluorescence recovery. Because a higher signal to noise ratio is inherent to the "turn on" or pre-adsorb strategy, the developed assay used GO/AuNPs composites that were preassembled before incubation with thrombin.

Unlike adsorption between dye-modified ssDNA and GO, unmodified AuNPs were easily adsorbed to GO in high ionic-strength buffers, although both were negatively charged (Fig. S1, ESI†). Strong van der Waals forces play a significant role in aggregation of AuNPs and GO through the screening of charge repulsions at high salt concentrations.[37] Accordingly, a moderate salt concentration is required to favor the adsorption of ssDNA to GO and avoid nonspecific adsorption of AuNPs to GO. To determine the most favorable ionic strength, the salt concentration was optimized. As shown in Fig. 1, the amount of AuNPs measured in the filtrate after incubating with GO in a PB buffer was found to vary with different concentrations of Mg^{2+} or Na^{+}. The difference was quantified by measuring the UV-Vis absorbance peak at 520 nm for 20 nm AuNPs. For 0.5 mM $MgCl_2$ (Fig. 1A), around 100% of the AuNP-TOEG6 (red circle, control group without ssDNA modification) was recovered in the filtrate after incubating with GO, indicated that there was no nonspecific binding between the AuNPs and GO. When the $MgCl_2$ concentration was higher than 1.0 mM, less than 70% of the AuNPs were recovered in the filtrate. The unrecovered AuNPs were non-specifically bound to the GO surface, so these conditions should be avoided. For all $MgCl_2$ concentrations, the aptamer modified AuNPs (black squares) were easily adsorbed to the GO surface and retained. Moreover, there was no aptamer modified AuNPs left in the filtrate after incubating with GO in the buffer solution with $MgCl_2$ concentration higher than 2.0 mM. Although the adsorption efficiency was not 100% under 0.5 mM $MgCl_2$ concentration, this concentration was optimal considering the nonspecific adsorption to the AuNPs without ssDNA. The

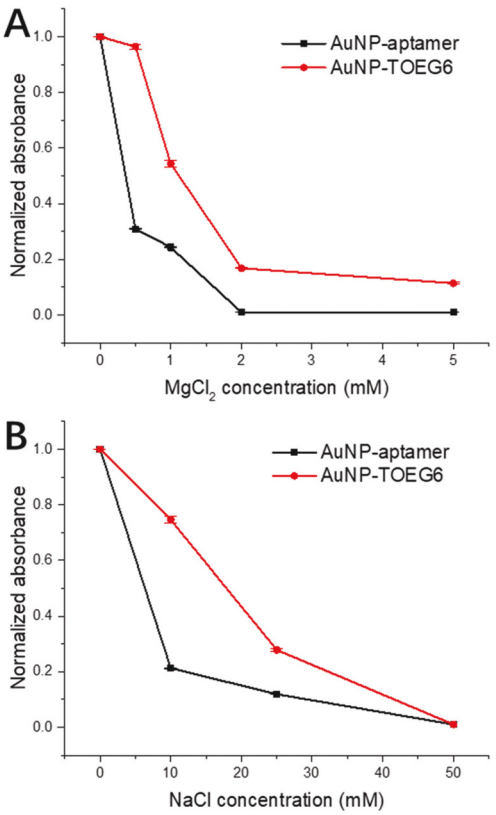

Fig. 1 UV-Vis absorption of AuNPs at 520 nm with different concentration of $MgCl_2$ (A) or NaCl (B). The AuNPs were in the filtrate after incubation with GO in a PB buffer (10.0 mM, pH 7.4).

same situation was also observed when using NaCl (Fig. 1B). However, the nonspecific adsorption still existed even when the concentration of NaCl was only 10.0 mM, which was much lower than the required concentration of Na^{+} for the interaction between ssDNA and GO.[38] Therefore, PB buffer with 0.5 mM $MgCl_2$ was chosen for the incubation of aptamer modified AuNPs and GO.

Formation of the composite was confirmed visually by 0.22 μm filtration at four stages of GO/AuNPs synthesis (Fig. 2). GO was retained on the filter membrane surface (brown color) because of its larger average size (>500 nm) than the membrane pore size (0.22 μm, Fig. 2A). The AuNPs–aptamer, which was only 20 nm in diameter, passed the membrane easily and no evidence of the residual AuNPs was seen on the membrane surface (Fig. 2B). When the GO/AuNPs composites formed by incubation of GO and AuNPs–aptamer, the residue on the membrane was a reddish brown color, resulting from the color of AuNPs on GO (Fig. 2C). The residue of the GO and AuNPs-TOEG6 (Fig. 2D) was the same as the pure GO (Fig. 2A), indicating no AuNPs nonspecifically adsorbed onto the GO. Formation of the GO/AuNPs composite was further confirmed by TEM images (Fig. S2C, ESI†). The GO was present in a classic one-layer sheet structure with the size larger than 500 nm. The 20 nm AuNPs (dark spots) were evenly distributed on the GO surface. No free AuNPs existed in the area without GO.

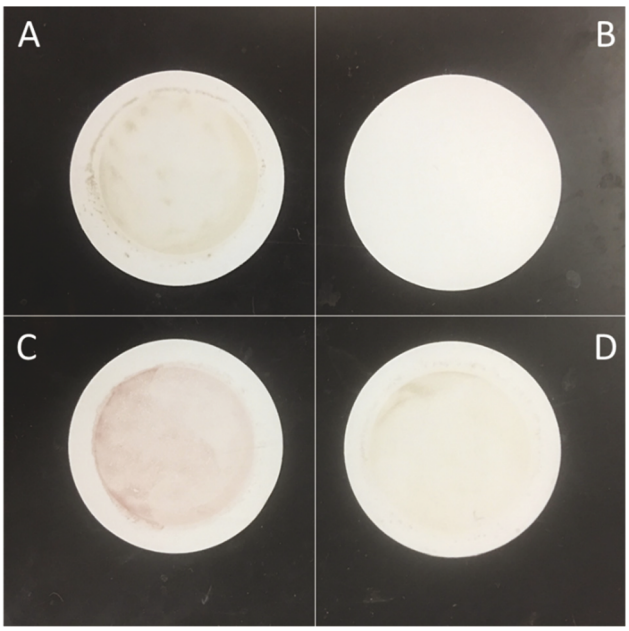

Fig. 2 Photos of GO/AuNPs collected on the filter membrane surface. A, GO only; B, AuNP–aptamer only; C, GO and AuNP–aptamer; D, GO and AuNP-TOEG6. Incubated in 1.0 mL of 10.0 mM PB buffer with 0.5 mM $MgCl_2$ (pH 7.4) for 10 min at room temperature. The GO concentration: 20 μg mL^{-1}; AuNPs concentration: 10^{10} nanoparticles per mL.

3.3. Validation of spICP-MS for ultrasensitive detection

The feasibility of ultrasensitive detection of AuNPs by spICP-MS was first verified. As shown in Scheme 1, the measured signal of the method is the number of desorbed AuNPs, which is proportional to the concentration of the target molecule. Solutions containing different number concentrations of standard AuNPs were tested using the spICP-MS. As shown in Fig. 3, the number of detected AuNPs (*i.e.*, measurements significantly greater than background) within 30 s systematically increased when the AuNP number concentration increased. The NP detection criterion applied in all measurements was signal (in counts) greater than five-times the baseline noise level. This noise level was 1 count, so a NP was detected if the signal intensity was higher than 5 counts. There were no detected NPs in the blank solution without AuNPs (Fig. 3A). By increasing the particle number concentration from 100 to 100 000 particles per mL, the number of NPs detected during the 180 s acquisition period increased from 2 to ~800 (Fig. 3B–G). The relationship between the number of detected NPs and the particle number concentration was calibrated under conditions of 0.20 μL min^{-1} flow rate and 6.45% transport efficiency. The results showed an excellent linear fit at a low concentration range (0–10 000 particles per mL, Fig. 3H inset). Hence, the number concentration of AuNPs in the solution could be absolutely quantified by using this calibration and the volume of the sample measured during the acquisition period. The number of AuNPs detected at high concentrations was lower than the expectation from the linear part of the calibration curve (Fig. 3H). This was probably by the greater likelihood of two AuNPs entering the plasma within one dwell time.

To demonstrate the greater capacity of spICP-MS for ultrasensitive assays using AuNPs, we compared the spICP-MS measurements of AuNP solutions with conventional ICP-MS measurements. For the later, an average $^{197}Au^{+}$ signal for many AuNPs (rather than a discreet signal from one AuNP) is measured because repeated sampling (10 sweeps) and a much a longer integration period (50 ms dwell time) is used. The results are listed in Table S2 (ESI†). The Au detection limit using conventional ICP-MS was 0.005 ppb, which was calibrated using gold standard solutions. There were no Au detected by conventional ICP-MS when the particle number concentration was lower than 10^6 particles per mL. In contrast, a solution of 100 particle per mL could be easily determined using the single particle mode with only a 3 min collection time. Note that the detection limit of the spICP-MS method could be even lower if the collection time was increased.[22] Moreover, the theoretical number of detected NPs calculated based on the literature[22] was close to the experimental data, demonstrating the reliability of the method. These data demonstrated that even if only a few hundred AuNPs desorbed from GO induced by a thrombin sample, they could be easily quantified by spICP-MS. Assuming each thrombin molecule of the 1 mL sample would desorb one AuNP and that each AuNP would be detected, this analytical performance would correspond to a thrombin concentration of less than 1×10^{-18} M.

3.4. Optimizations

Unlike the dye-based signaling molecules used in fluorescence bioassays, there are numerous positions on AuNPs that can be bound with ssDNA when used for signaling in spICP-MS bioassays. The high loading capacity of ssDNA on AuNPs can strengthen the interaction between the modified AuNPs and GO. However, heavily modified AuNPs can become too hard to desorb in the presence of target. Hence, the ssDNA density on the AuNPs, which would affect the desorption efficiency of ssDNA in the thrombin, was optimized prior to the detection. TOEG6, a protein-repellent alkanethiol, was used to stabilize the AuNPs by passivating the particle surface during the ssDNA immobilization. The amount of ssDNA on the AuNPs surface was tuned by changing the ratio of ssDNA to TOEG6.[35] The exact amount of ssDNA was quantified by measuring the supernatant fluorescence of Alex-750 appended to the free end of the thrombin aptamer. The ssDNA density on AuNPs at different concentrations of TOEG6 is summarized in Table S3 (ESI†). The higher the TOEG6 concentration, the lower ssDNA density on the AuNPs. Finally, an average of one ssDNA per particle was obtained when the TOEG6 concentration increased to 15 μM, which was 60-times higher than the ssDNA concentration. After obtaining aptamer-modified AuNPs with different numbers of immobilized ssDNA, the assay was optimized based on the number of AuNPs detected by spICP-MS. As shown in Fig. 4A, the number of detected AuNPs increased with decreasing number of immobilized

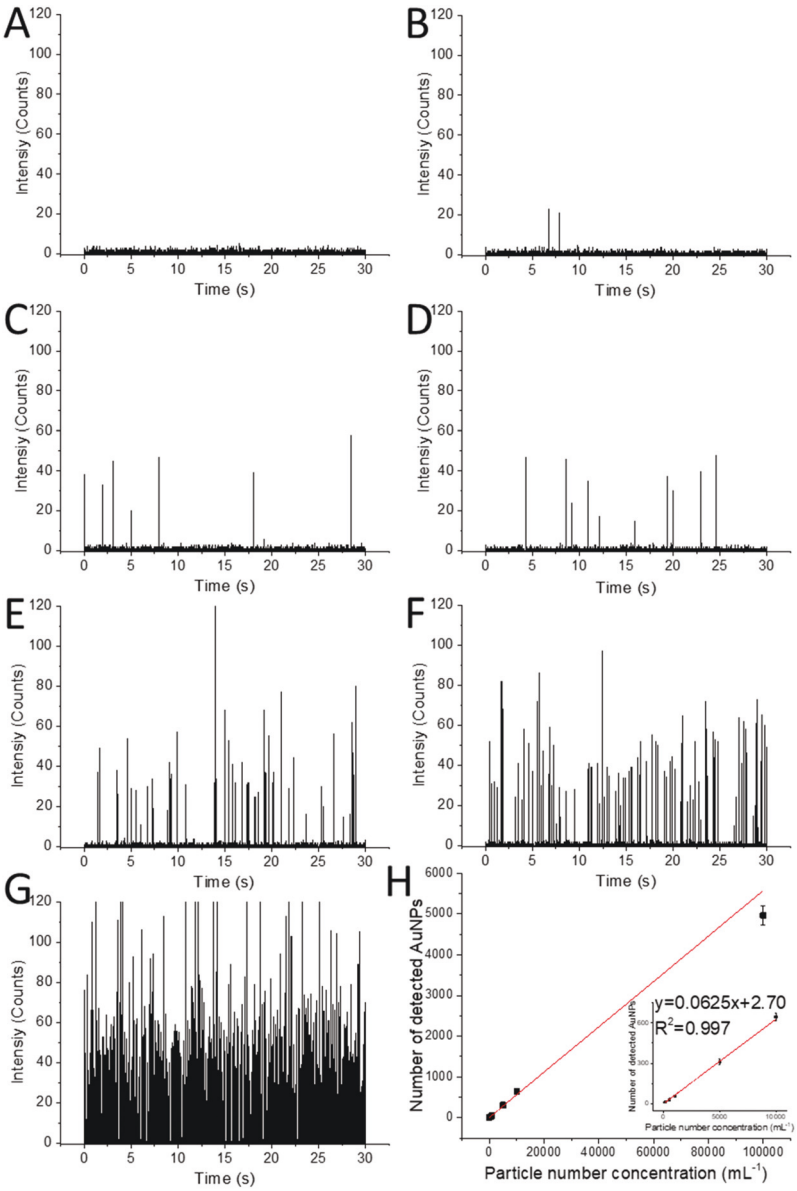

Fig. 3 spICP-MS spectra of AuNPs in different particle number concentrations. A–G: 0, 100, 500, 1000, 5000, 10 000, and 100 000 particles per mL (^{197}Au, dwell time: 5 ms). H. Relationship between the number of detected AuNPs and the particle number concentration from 0 to 100 000 particles per mL within 180 s collection time. Inset: Calibration curve of the number of detected AuNPs and the particle number concentration from 0 to 10 000 particles per mL.

ssDNA, demonstrating that AuNPs with less immobilized aptamer would more easily desorb from the GO surface under the same concentration of thrombin. To achieve the best result, AuNPs with an average of one ssDNA per particle was chosen as the optimum aptamer modified AuNP reagent. Some of the AuNPs might contain no ssDNA; however, this would not affect the assay because those AuNPs without ssDNA could be washed out by passing the filter membrane before introducing to the target molecules. The results in Fig. 2 support that these AuNPs with TOEG6 had little attraction with the GO.

To guarantee that the reaction of thrombin with aptamer reached equilibrium before spICP-MS analysis, the incubation time of thrombin and GO/AuNPs composites was investigated. As shown in Fig. 4B, the number of detected NPs increased quickly with incubation time during the first 30 min but reached a plateau at 60 min. There was no further change even when the incubation time was extended to 2 h. As a result, the incubation time of 60 min was determined as the optimal reaction time for the assay method.

3.5. Sensitivity to thrombin concentration

The assay was applied to thrombin determination using the spICP-MS under the optimized conditions. As shown in Fig. 5, the number of detected AuNPs systematically increased within the 30 s collection time as the thrombin concentration

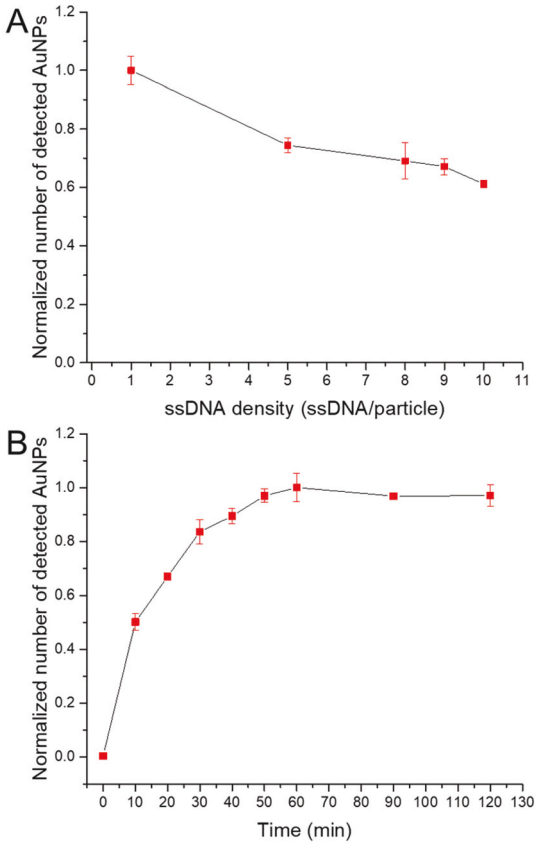

Fig. 4 The optimizations of aptamer density on AuNPs (A), and incubation time (B). Thrombin concentration: 10 pM. GO/AuNPs composites concentration: 1 μg mL^{-1} (GO mass based) incubation in PBS buffer (10 mM with 0.5 mM $MgCl_2$, pH 7.4).

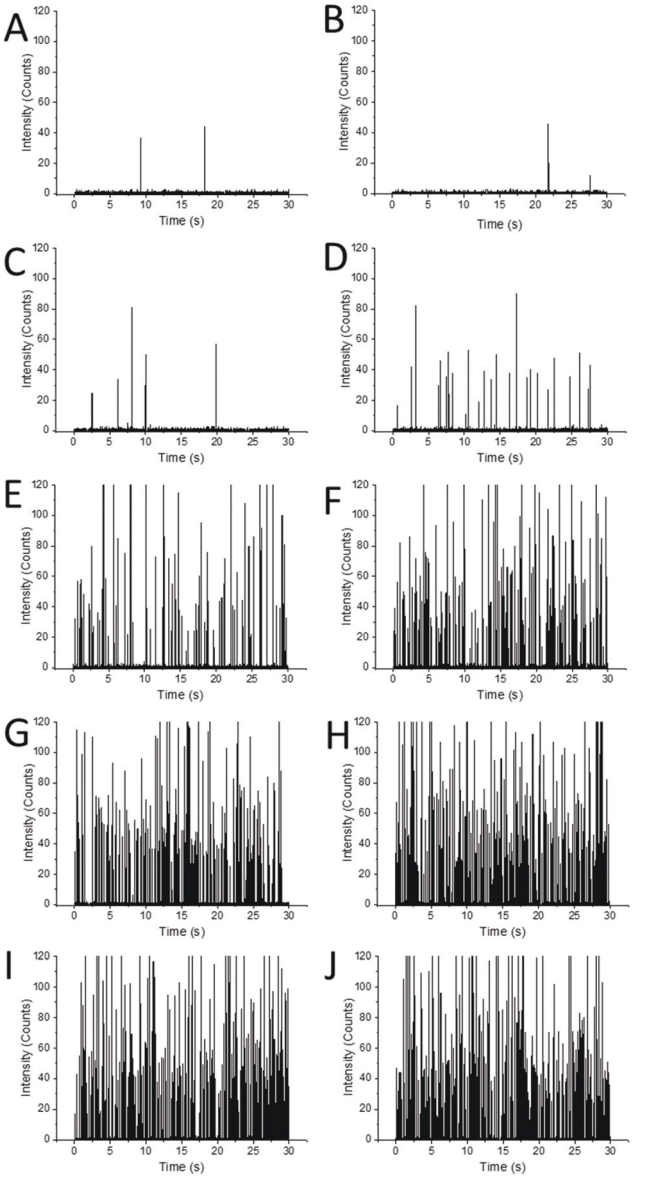

Fig. 5 spICP-MS spectra of AuNPs in the presence of different concentrations of thrombin (A to J: 0, 10^{-4}, 10^{-3}, 10^{-2}, 10^{-1}, 1, 10, 10^2, 10^3, 10^4 pM). GO/AuNPs composites concentration: 1 μg mL^{-1} (GO mass based). Incubation at 37 °C for 60 min in PBS buffer (10 mM, 0.5 mM $MgCl_2$, pH 7.4). 200 folds dilution before injecting into spICP-MS (^{197}Au, dwell time: 5 ms).

increased from 1.0 fM to 10.0 nM. There were also a few detected AuNPs without adding thrombin in the blank (Fig. 5A). The concentration of residual AuNPs in the blank was as high as $(40 \pm 6) \times 10^3$ particle per mL after washing steps. Moreover, there was no difference between the blank sample and the sample with 0.1 fM of the thrombin, which established a concentration below the detection limit of the method (Fig. 5B). With the 1.0 fM of thrombin sample, there was a noticeable increase in detected AuNPs compared with blank, although the distinction was only slight (Fig. 5C). When the concentration of thrombin was higher than 10.0 fM, the number of detected AuNPs increased dramatically (Fig. 5D–J).

The quantitative relationship between the concentration of thrombin and the concentration of desorbed AuNPs is demonstrated in Fig. 6. Here, N_0 is the number of detected AuNPs in the blank as control and N is the number of detected AuNPs at different thrombin concentrations. This assay showed a broad dynamic range from 1.0 fM to 10.0 nM. It also showed a logarithmic relationship with the thrombin concentration from 10.0 fM to 100.0 pM (Fig. 6 inset) with a correlation coefficient (R^2) of 0.9997. The limit of detection was estimated to be 4.5 fM by the 3σ rule, which was around five orders of magnitude lower than the similar graphene based fluorescence platform.[6,10]

3.6. Selectivity

The specificity of the developed sensor was evaluated by testing other protein components in a serum sample. As shown in Fig. 7, the desorbed AuNPs detected by reacting with BSA, IgG, and FBS respectively at a concentration of 1.0 μM (~0.1 g protein per L for FBS) were less than 10% of that caused by thrombin at a concentration of 10.0 pM. This result strongly demonstrated that the method could be used for both selective and sensitive detection of the target biomolecules. Moreover, based on the recovery measurement for FBS sample spiked with 10 pM of thrombin (recovery: 117 ± 13%), the fact

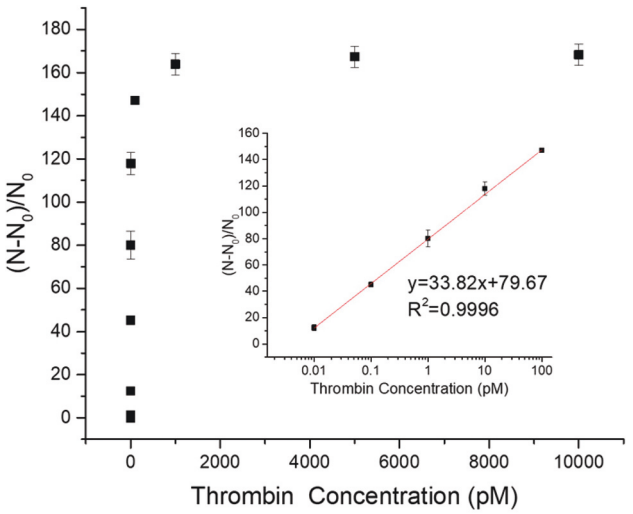

Fig. 6 Relationship between the changes of number of detected AuNPs and thrombin in concentration from 10^{-4} to 10^{4} pM. Acquisition period: 180 s. Inset: Calibration curve of the changes of number of detected AuNPs and thrombin concentration from 10^{-2} to 10^{2} pM.

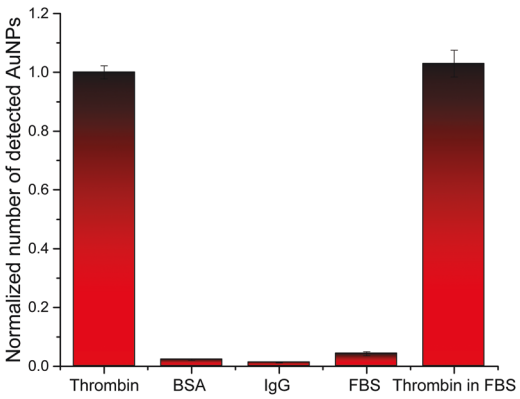

Fig. 7 Selectivity of the platform for thrombin detection by spICP-MS. Thrombin concentration: 10.0 pM; BSA and IgG concentrations: 1.0 μM; FBS concentration: ~0.1 g protein per L. GO/AuNPs composites concentration: 1 μg mL^{-1} (GO mass based). Incubation at 37 °C for 60 min in PBS buffer (10 mM, 0.5 mM $MgCl_2$, pH 7.4).

that the sample of thrombin in FBS showed the same signal level compared to the pure thrombin showed that the method was not significantly influenced by interferences and indicated its great potential for applications with complex sample interferes.

4. Conclusions

An effective and versatile GO/AuNPs platform for ultrasensitive detection of target biomarkers using spICP-MS technology was developed. In this case, thrombin was used as a model target biomarker and could be detected at as low concentration as 4.5 fM. Compare with similar fluorescence-based platforms this detection limit was lower by five orders of magnitude, making this method comparable to other ultrasensitive methods for thrombin.[39,40] It is also noteworthy that this detection limit could be further reduced by removing the free AuNPs in the GO/AuNPs composites or coupling an amplification strategy. Because of the excellent specificity of the aptamer,[32] this platform also showed high selectivity. Moreover, the type nanoparticles used as a metal isotope signal for spICP-MS could be varied, making it possible for simultaneous detection of multiple biomarkers if a time-of-flight mass spectrometer was employed. Finally, the method's minimal interference from the matrix makes it suitable for applications in clinical diagnostics.

Conflicts of interest

There are no conflicts to declare.

Acknowledgements

This work was supported by the NSF grant CHE 1709160 and NSF EPSCoR RII Track 1 Cooperative Agreement 1946202 (J. X. Z.), UND Applied Research to Address the State's Critical Needs Initiative program (X.W.) and the NIH grant 5P20GM103442-18 (D.T.P). The authors acknowledge the use of the Edward C. Carlson Imaging and Image Analysis Core Facility which is supported in part by NIH grant 1P20GM113123 and P20GM103442 and also acknowledge use of the North Dakota INBRE Metal Analysis Core Facility, which is supported in part by NIH grant 5P20GM103442-18.

References

1 X. Wu, F. Mu, Y. Wang and H. Zhao, *Molecules*, 2018, **23**, 2050.
2 Y. Liu, X. Dong and P. Chen, *Chem. Soc. Rev.*, 2012, **41**, 2283–2307.
3 X. Huang, Z. Yin, S. Wu, X. Qi, Q. He, Q. Zhang, Q. Yan, F. Boey and H. Zhang, *Small*, 2011, **7**, 1876–1902.
4 J. Kim, L. J. Cote and J. Huang, *Acc. Chem. Res.*, 2012, **45**, 1356–1364.
5 Z. Liu, B. Liu, J. Ding and J. Liu, *Anal. Bioanal. Chem.*, 2014, **406**, 6885–6902.
6 C. H. Lu, H. H. Yang, C. L. Zhu, X. Chen and G. N. Chen, *Angew. Chem., Int. Ed.*, 2009, **48**, 4785–4787.
7 P. Alonso-Cristobal, P. Vilela, A. El-Sagheer, E. Lopez-Cabarcos, T. Brown, O. L. Muskens, J. Rubio-Retama and A. G. Kanaras, *ACS Appl. Mater. Interfaces*, 2015, **7**, 12422–12429.
8 M. Li, X. Zhou, S. Guo and N. Wu, *Biosens. Bioelectron.*, 2013, **43**, 69–74.
9 Y. He, Y. Lin, H. Tang and D. Pang, *Nanoscale*, 2012, **4**, 2054–2059.

10 H. Chang, L. Tang, Y. Wang, J. Jiang and J. Li, *Anal. Chem.*, 2010, **82**, 2341–2346.
11 M. Zhang, B. C. Yin, W. Tan and B. C. Ye, *Biosens. Bioelectron.*, 2011, **26**, 3260–3265.
12 Y. Wang, Z. Li, J. Wang, J. Li and Y. Lin, *Trends Biotechnol.*, 2011, **29**, 205–212.
13 J. Pena-Bahamonde, H. N. Nguyen, S. K. Fanourakis and D. F. Rodrigues, *J. Nanobiotechnol.*, 2018, **16**, 75.
14 Y. Wu, R. D. Tilley and J. J. Gooding, *J. Am. Chem. Soc.*, 2018, **141**, 1162–1170.
15 Y. Zhao, F. Chen, Q. Li, L. Wang and C. Fan, *Chem. Rev.*, 2015, **115**, 12491–12545.
16 E. Vermisoglou, D. Panáček, K. Jayaramulu, M. Pykal, I. Frébort, M. Kolář, M. Hajdúch, R. Zbořil and M. Otyepka, *Biosens. Bioelectron.*, 2020, **166**, 112436.
17 J. Anna, J. Aleksandra, K. Mateusz, B. Sylwia and P. Barbara, *Curr. Med. Chem.*, 2019, **26**, 6878–6895.
18 W. Wang, H. Su, Y. Wu, T. Zhou and T. Li, *J. Electrochem. Soc.*, 2019, **166**, B505–B520.
19 M. D. Montano, J. W. Olesik, A. G. Barber, K. Challis and J. F. Ranville, *Anal. Bioanal. Chem.*, 2016, **408**, 5053–5074.
20 C. Degueldre and P. Y. Favarger, *Colloids Surf., A*, 2003, **217**, 137–142.
21 F. Laborda, E. Bolea and J. Jimenez-Lamana, *Anal. Chem.*, 2014, **86**, 2270–2278.
22 F. Laborda, J. Jiménez-Lamana, E. Bolea and J. R. Castillo, *J. Anal. At. Spectrom.*, 2013, **28**, 1220–1232.
23 F. H. Lin, S. I. Miyashita, K. Inagaki, Y. H. Liu and I. H. Hsu, *J. Anal. At. Spectrom.*, 2019, **34**, 401–406.
24 A. R. Montoro Bustos, E. J. Petersen, A. Possolo and M. R. Winchester, *Anal. Chem.*, 2015, **87**, 8809–8817.
25 R. Peters, Z. Herrera-Rivera, A. Undas, M. van der Lee, H. Marvin, H. Bouwmeester and S. Weigel, *J. Anal. At. Spectrom.*, 2015, **30**, 1274–1285.
26 J. Hu, D. Deng, R. Liu and Y. Lv, *J. Anal. At. Spectrom.*, 2018, **33**, 57–67.
27 G. Han, Z. Xing, Y. Dong, S. Zhang and X. Zhang, *Angew. Chem., Int. Ed.*, 2011, **50**, 3462–3465.
28 S. Zhang, G. Han, Z. Xing, S. Zhang and X. Zhang, *Anal. Chem.*, 2014, **86**, 3541–3547.
29 S. O. Kelley, *ACS Sens.*, 2017, **2**, 193–197.
30 A. Bini, M. Minunni, S. Tombelli, S. Centi and M. Mascini, *Anal. Chem.*, 2007, **79**, 3016–3019.
31 R. C. Becker, *J. Thromb. Thrombolysis*, 2005, **19**, 71–75.
32 M. Ilgu and M. Nilsen-Hamilton, *Analyst*, 2016, **141**, 1551–1568.
33 L. Yan, J. Zhou, Y. Zheng, A. S. Gamson, B. T. Roembke, S. Nakayama and H. O. Sintim, *Mol. Biosyst.*, 2014, **10**, 970–1003.
34 Y. Liu, N. Liu, X. Ma, X. Li, J. Ma, Y. Li, Z. Zhou and Z. Gao, *Analyst*, 2015, **140**, 2762–2770.
35 J. Deka, R. Mech, L. Ianeselli, H. Amenitsch, F. Cacho-Nerin, P. Parisse and L. Casalis, *ACS Appl. Mater. Interfaces*, 2015, **7**, 7033–7040.
36 J. Lee, J. Kim, S. Kim and D. H. Min, *Adv. Drug Delivery Rev.*, 2016, **105**, 275–287.
37 J. Liu, *Phys. Chem. Chem. Phys.*, 2012, **14**, 10485–10496.
38 M. Wu, R. Kempaiah, P. J. Huang, V. Maheshwari and J. Liu, *Langmuir*, 2011, **27**, 2731–2738.
39 Y. Zhang, J. Xia, F. Zhang, Z. Wang and Q. Liu, *Sens. Actuators, B*, 2018, **267**, 412–418.
40 C. Wang, Y. Qian, Y. Zhang, S. Meng, S. Wang, Y. Li and F. Gao, *Sens. Actuators, B*, 2017, **238**, 434–440.